Collision, Adhesion, and Oxidation of Single Ag Nanoparticles on a Polysulfide-Modified Microelectrode

Peter A. Defnet and Bo Zhang*

Department of Chemistry, University of Washington, Seattle Washington United States 98195-1700

Corresponding author, zhangb@uw.edu

Abstract. We report the collision, adhesion, and oxidation behavior of single silver nanoparticles (Ag NPs) on a polysulfide-modified gold microelectrode. Despite its remarkable success in volume analysis for smaller Ag NPs, the method of NP-collision electrochemistry has failed to analyze particles greater than 50 nm due to uncontrollable collision behavior and incomplete NP oxidation. Herein we describe the unique capability of an ultrathin polysulfide layer in controlling the collision behavior of Ag NPs by drastically improving their sticking probability on the electrode. The ultrathin sulfurous layer is formed on gold by sodium thiosulfate electro-oxidation and serves both as an adhesive interface for colliding NPs and as a preconcentrated reactive medium to chemically oxidize Ag to form Ag_2S. Rapid particle dissolution is further promoted by the presence of bulk sodium thiosulfate serving as a Lewis base, which drastically improves the solubility of generated Ag_2S by a factor of 10^{13}. The combined use of polysulfide and sodium thiosulfate allows us to observe a 25x increase in NP detection frequency, 3x increase in peak amplitude, and more complete oxidation for larger Ag NPs. By recognizing how volumetric analysis using transmission electron microscopy (TEM) may overestimates quasi-spherical NPs, we believe we can have full NP oxidation for particles up to 100 nm. By focusing on the electrode/solution interface for more effective NP-electrode contact, we expect that the knowledge learned from this study will greatly benefit future NP collision systems for mechanistic studies in single-entity electrochemistry as well as designing ultrasensitive biochemical sensors.

Introduction:

A basic heterogeneous electron-transfer (ET) event can take place when a redox molecule, such as ferrocene, diffuses and collides on the surface of the electrode biased at an appropriate potential. A freely-diffusing metal nanoparticle (NP), such as silver, may also collide and transiently oxidize on the electrode surface transferring many electrons within a short period of time, e.g., a few μs. The process of single NPs colliding and interacting with the electrode, however, can be drastically different from that of small redox molecules, as recently revealed in the electrochemistry literature. Starting from early 2000s, NP collision electrochemistry has grown to a new and broad field studying the reactivities and mechanisms for individual NPs interacting with electrodes.[1,2] Collision dynamics depend on the reactivity of the NP, the redox species, and the underlying electrode material. For example, an inert particle adsorbing on the electrode may partially block the flux of the redox species resulting in a reduction in the faradaic signal.[3] A catalytic NP, on the other hand, may enhance the faradaic signal when it adsorbs onto a more insert electrode.[4] A third situation arises when a more reactive NP (often metal, such as silver or gold) collides on the electrode surface and becomes oxidized causing a transient positive-going current signal due to particle oxidation and dissolution.[5] Because the charge transferred during the collision event can be quantitatively related to the number of Ag atoms oxidized from the Faraday's law, the method of Ag NP collision may be used as a high throughput approach for single-particle volume analysis.[6,7]

Ag NPs have been well-studied for many applications including therapeutics, optical sensors, and consumer products.[8,9] Small variations in size, shape, and volume can significantly influence their chemical properties, including reactivity, and toxicity.[10,11] Accurate size-characterization techniques are therefore necessary for well-controlled experimentation. However, traditional methods such as transmission electron microscopy (TEM) and dynamic light scattering (DLS) struggle to accurately quantify the volume for non-ideal NP geometries, particularly when irregularities or defects are present.[12] Electron tomography may alternatively be used; however, this technique requires long analysis times with expensive instrumentation, thereby making it cost-prohibitive to measure a statistically relevant number

of samples for multiple populations.[13] Instead, the electrochemical method of NP collision has shown great promise toward Ag NP volumetric determination.[14]

Despite its enormous potential for single particle analysis, a key challenge of NP collision has been the poor control over how a NP interacts with the electrode and the observation of incomplete NP oxidation, especially for large-size particles. For example, several studies in 2017 demonstrated the incomplete oxidation of Ag NP's over 50 nm in diameter, highlighting the limits of the technique.[15–17] Mechanistic studies revealed a multipeak signal proposed to be from NPs rapidly bouncing across the electrode surface.[15–17] Simulations have suggested that the NP only contacts the UME in rapid nanosecond-scale bursts due to its fast diffusional motion.[18] These studies utilized neutral electrolyte conditions and cited NP diffusion away from the electrode as the principle mechanisms for partial oxidation.[19]

The challenge in controlling NP-electrode interaction was recently tackled by Long and co-workers, who reported the use of an adhesive NP-UME mechanism.[20] Their work used a bare Au electrode and an alkaline phosphate condition to record Ag NP collision. The authors believed that a layer of Ag oxide forms *in-situ* during particle collision and is responsible for promoting particle adhesion. Amperometric peaks with long 20 ms decays were reported due to the slow dissolution of adsorbed Ag oxide. However, their main figures and supporting data show very broad distributions of oxidation efficiencies for 65 nm diameter NPs, suggesting not all colliding NPs underwent complete oxidation. Similarly broad trailing distributions were obtained in a separate publication from Long and co-workers utilizing the same electrolyte condition for 60 nm Ag NPs.[21]

In this work, we demonstrate how NP collision, adhesion, and oxidative dissolution can be dramatically promoted by the use of an adhesive polysulfide layer and the use of thiosulfate electrolyte as a Lewis base. An ultrathin layer of polysulfide (S^0) is formed on the Au surface from a unique surface-adsorbed electrochemical pathway in alkaline sodium thiosulfate, described in Equation 1.[22]

$$S_2O_3^{2-} + H_2O \leftrightarrows S^0 + SO_4^{2-} + 2H^+ + 2e^- \quad (1)$$

The polysulfide is sufficiently thin to permit Ag oxidation via electron tunneling,[22,23] while at the same time promotes Ag NP adhesion due to the strong Ag-S interaction.[24] For example, Pakiari and Jamshidi estimated that the strength of Ag-S bonds is an impressive 25% of the notoriously strong Au-S bonds.[25] The strong Ag-S bond has also extensively been used to functionalize Ag NPs with organic and biological molecules.[26–29] Thus, single Ag NPs collide and stick to the adhesive polysulfide film while undergoing electro-oxidation.

Our results suggest that the polysulfide layer directly reacts with Ag NPs to form Ag_2S, thus improving the rate of oxidation over diffusion-controlled systems. Despite the high insolubility of Ag_2S,[30] the use of bulk sodium thiosulfate as a Lewis base vastly increases the solubility of silver salts via formation of a metal complex ($K_f = 1.7 \times 10^{13}$ for $Ag(S_2O_3)_2^{3-}$); see S12 for details. In a direct comparison with control studies, we find up to a 25x increase in collision frequency, 3x increase in peak amplitude, and more accurate quantitation for 60 nm Ag NPs. Volumetric measurements are compared between 30, 40, 60, 80, and 100 nm populations sized using NP collision data and TEM. By acknowledging that TEM overestimates quasi-spherical NP volumetric measurements, as explained in detail later, our results demonstrate the possibility of full NP oxidation up to 100 nm diameter. Mechanistic implications are further discussed to explain the manner in which this simple methodology so dramatically improves the electron transfer behavior of colliding Ag NPs.

Experimental:

Chemicals. All chemicals were used as received from the manufacturer and include sodium thiosulfate pentahydrate ($Na_2S_2O_3 \cdot 5H_2O$, 100%, Fisher Chemical), sodium hydroxide (NaOH, 98.5%, J.T. Baker), potassium chloride (KCl, 100%, Fisher Chemical), ferrocenemethanol (FcMeOH, 97%, Sigma Aldrich), and sodium citrate dihydrate (100%, J.T. Baker). Commercial Ag nanoparticles with 30, 40, 60, 80, and

100 nm diameters stored in 2 mM trisodium citrate were purchased from Nanocomposix (San Diego, CA). Solutions were prepared with nanopure water purified to a resistivity of 18.2 MΩ cm^{-1} (Barnstead Nanopure system, Thermo Scientific).

Electrode Preparation. The 25-µm diameter Au disc UMEs were fabricated as previously reported.[16] Electrodes were screened for ideal voltammetric behavior using cyclic voltammetry in 1 mM FcMeOH and 100 mM KCl. UMEs were freshly polished with fine sandpaper and rinsed with excess DI water prior to all experiments. Ag/AgCl quasi-reference electrodes were prepared by immersing Ag wire (99.99% Alfa Aesar) in bleach for at least 1 hour. All collision experiments were performed with freshly chlorided and coiled wires.

Instrumentation. Chronoamperometric NP collision traces were collected using a low-noise current amplifier with an internal low-pass filter of 10 kHz (Axopatch 200B, Molecular Devices) and digitized with high temporal resolution at a sampling rate of 100 kHz (DigiData 1440b). Amperometric measurements were recorded within two home-built faraday cages located on a vibration isolation table. Each cage was externally grounded and closed. The internal faraday cage rested on thick 6" foam padding to further isolate vibrations due to movement in the surrounding area. Amperometric traces were recorded with Axoscope 11.1 software and analyzed using a custom Python script as described in **S1**.

Cyclic voltammograms (CVs) were recorded using a LabVIEW program created in-house. Potential was swept with an external potentiostat (EG&G Parc Model 175) and high sensitivity current was measured with a Chem-Clamp current amplifier (Dagan Corporation). CVs were recorded within a grounded and closed home-built faraday cage resting on top of thick foam padding.

Single Nanoparticle Collision Experiments. NP collision experiments were performed in 5 mL volumes for each reported electrolyte condition. The 25 µm Au UME and Ag/AgCl quasi-reference electrodes were dipped in the electrolyte solution and leads applying +600 mV were connected while recording the amperometric current.

For the "thiosulfate with sulfide" condition in **Figures 3, 4 and 5**, the solution consisted of 10 mM $Na_2S_2O_3$ 10 mM NaOH. A potential pulse was used to modify the electrode with the polysulfide

layer. It was experimentally found that switching the potential from 600 mV to 0 V for 30 seconds and back to 600 mV invoked the polysulfide passivation process *in-situ*, evidenced by current overloading as shown in **Figure 2b**. We note that the same bulk electrolyte was used for both the modification process and for the Ag NP detection. The "thiosulfate without sulfide" condition in **Figures 3 and 4** also consisted of 10 mM $Na_2S_2O_3$ 10 mM NaOH but did not employ the potential pulse and did not observe overloading current, indicative of the absence of the polysulfide layer. The "alkaline KCl" (10 mM KCl 10 mM NaOH) and "neutral KCl" (20 mM KCl) conditions in **Figures 3 and 4** did employ the potential pulseto maintain consistency, but no effect was observed as the current immediately decayed to near 0 pA.

Once the current decayed to a flat baseline near 0 pA for each condition, 300 µL of stock Ag NPs were injected and mixed into the solution. The resulting diluted Ag NP concentrations for each NP size are displayed in S2.

The solution concentration of 10 mM $Na_2S_2O_3$ 10 mM NaOH was selected following parameter optimization to both avoid NP aggregation and facilitate ease of recording. A more detailed discussion is included in S3.

We note that all reported electrolyte solutions contained 120 µM citrate due to the presence of 2 mM citrate within the injected NP aliquot. The solutions used for cyclic voltammetry in **Figure 1a** and **S4** were spiked with the same citrate concentration to maintain consistency.

Nanoparticle Characterization. TEM was performed using a FEI Technai G2 F20 TEM operating at 200 kV with a single tilt sample holder and Gatan Ultrascan CCD camera. The 30, 40, 60, 80, and 100 nm Ag NP's were each dropcast onto separate carbon-coated copper TEM grids (Electron Microscopy Sciences). The TEM images were analyzed with the 2-D projection method, outlined in S5, to provide an estimated equivalent spherical diameter distribution for NP's of each sample.

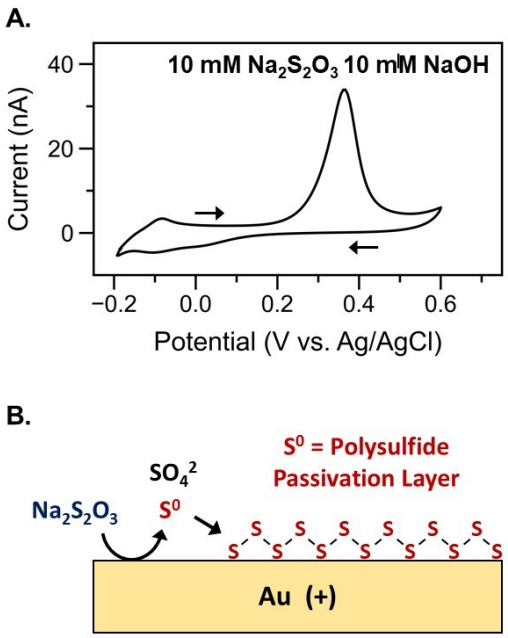

Figure 1. Surface Modification of Bare Au Electrode with Polysulfide. **(A)** A cyclic voltammogram in 10 mM $Na_2S_2O_3$ 10 mM NaOH swept from -0.2 V to 0.6 V to -0.2 V at 20 mV/s vs. Ag/AgCl. The large oxidation wave at 0.35V is due to thiosulfate oxidation. The rapid decline in current at 0.45 V is due to the passivation of the UME with the polysulfide layer, preventing further thiosulfate oxidation. The second cycle is shown, although we note that continued cycling produces nearly identical waveforms as shown in S4A. **(B)** A qualitative representation of the mechanism described in Equation 1, where the oxidation of alkaline thiosulfate results in the formation of a polysulfide passivation layer across the Au electrode surface.

Results and Discussion:

Thiosulfate Electrochemistry and the Polysulfide Passivation Process. The electrochemistry of alkaline thiosulfate on Au undergoes multiple reaction pathways depending on applied potential. Previous literature utilizing surface-enhanced Raman spectroscopy (SERS) has revealed the composition of surface adsorbed species under various conditions.[31,32] Two reaction pathways are of significant interest to the present study. First, the Au electrode undergoes leaching with the thiosulfate between 0 and 0.1 V vs. Ag/AgCl, thereby promoting its own dissolution.[31] A monolayer of Au sulfide begins to form after long exposure, where a fractional coverage of 0.35 was reported after 18 minutes at 0.1 V in 100 mM $Na_2S_2O_3$.[31] Second, as the potential is increased beyond 0.45 V, thiosulfate oxidation occurs at the Au

electrode and produces a thin film of adsorbed S-S bonds existing as cyclo-octa sulfur (S_8) or polysulfide (Equation 1).[22] The polysulfide film passivates the Au electrode and inhibits continued leaching or further oxidation of thiosulfate.[33]

We represent the passivation process schematically in **Figure 1b** and qualitatively reproduce the cyclic voltammetry results in **Figure 1a** for our thiosulfate NP collision condition. After scanning the potential from -0.2 V to 0.7 V to -0.2 V, we observed that the leaching current at 0.1 V is almost negligible. The thiosulfate oxidation wave dominates the trace and peaks at 0.36 V with 34 nA and is followed by the expected rapid current decay indicative of electrode passivation with polysulfide. On the reverse scan, reduction of the film begins at -0.2 V.

The sulfide film has been well-studied and has a set of known conditions required for its formation and stability. For example, the film's generation and electrode passivation is unique to Au, and specifically does not occur on other commonly used electrode materials including glassy carbon, Ag, and Pt. Further, its formation via the thiosulfate pathway requires alkaline conditions to avoid the acidic decomposition of thiosulfate in solution.[34] Once generated, the film is relatively stable at potentials ranging from +0.8 V to -0.2 V vs. Ag/AgCl where its own reduction begins to occur, as shown in **Figure 1a**.[35]

Previous literature suggests that the application of potentials above 0.45 V vs. Ag/AgCl would invoke thiosulfate oxidation and subsequent electrode passivation. In our amperometric experiments, thiosulfate oxidation was readily evident by the immediate overloading of the background current. The overloaded signal would occur for a few minutes before rapidly decaying back to ~ 0 pA, indicative of electrode passivation. However, occasionally initialization of the potential at +0.6 V in 10 mM $Na_2S_2O_3$ 10 mM NaOH solution did not generate an anodic current. This phenomenon was also observed in cyclic voltammetry where potential onset at +0.3 V scanning positively to +0.7 V sometimes produced a flat signal. Only upon cycling back down through 0 V was this oxidation wave induced. To overcome this inconsistency in our amperometric recordings and generate a reproducible polysulfide film, we applied a single potential pulse between +0.6 V to 0 V to +0.6 V prior to our NP collision experiments. This

modification process generated a consistent overloading background current that decayed back to ~ 0 pA after 4-5 minutes.

It remains unclear as to why sweeping the potential through 0 V is required to consistently generate the passivating film. We speculate that formation of Au-sulfide nucleation zones may better anchor the film to the electrode surface, yet this would not explain the absence of anodic current. It may also be possible that freshly exposed Au following leaching may remove oxide impurities and be more reactive. Further studies with correlated spectroscopy would be required to better understand this behavior.

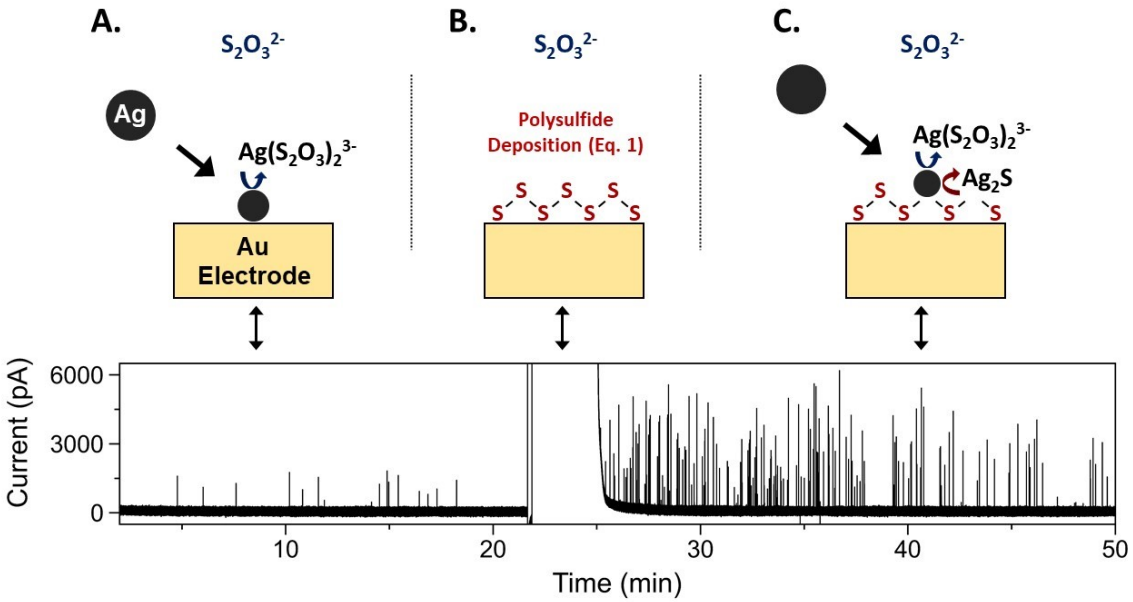

Figure 2: Correlated Mechanism and Amperometric Trace for Polysulfide Ag NP Collisions. The entire trace above was recorded in 10 mM $Na_2S_2O_3$ 10 mM NaOH with 60 nm diameter Ag NPs at 19 pM. **(A)** For the first ~20 minutes, particles collide onto a bare Au UME, forming $Ag(S_2O_3)_2^{3-}$ as a stable product. **(B)** Polysulfide is deposited onto the Au UME with application of a single potential pulse, as outlined in the text. Overloading current is from $Na_2S_2O_3$ oxidation and polysulfide deposition, as described in Equation 1. **(C)** A stable baseline is achieved following polysulfide passivation. The sulfide adheres colliding NPs and can directly react to form Ag_2S.

Effects of Polysulfide Modification on Ag NP Collision. In **Figure 2** we demonstrate the qualitative effects of employing the polysulfide layer on the Ag NP collision results. The trace was recorded in 10 mM $Na_2S_2O_3$ 10 mM NaOH with 19 pM diffuse 60 nm diameter Ag NPs. The first ~20 minutes (**Figure 2a**) were recorded without the sulfide layer present, evidenced by the absence of anodic overloading

current prior to NP injection; here we observed small infrequent peaks. At ~20 minutes (**Figure 2b**) the potential was pulsed to 0 V for 30 seconds and back to 600 mV to invoke the polysulfide modification, evidenced by the current overloading. The residual current decayed to the original ~ 60 pA within minutes following the modification procedure. With the polysulfide layer present, the NP collision signal was dramatically changed as shown in **Figure 2c**. We observed large rapid peaks with a 9x increase in average collision frequency and 2.5x increase in average amplitude.

Closer inspection of the non-sulfide peaks reveals single collision events with 3x longer durations which indicate slower electron transfer kinetics. However, the absence of multipeaks suggests NP adhesion, possibly bound to interfacial layers of adsorbed thiosulfate[22] or sparse coverage of sulfurous thiosulfate decomposition products.[35] Herein, we propose two related interfacial mechanisms that help to explain the disparate Ag NP collision results with and without the polysulfide layer present.

One mechanism for taller, faster peaks is that colliding Ag NPs can directly react with the polysulfide film to form Ag_2S. The preconcentrated sulfide serves as a precursor toward the stable oxidation product, Ag_2S, as described in Equation 2.

$$2Ag + S^0 \leftrightarrows Ag_2S\ (s) \qquad (2)$$

The solid Ag_2S layer formed at the contact position can then react with the bulk thiosulfate to form $Ag(S_2O_3)^{2-}$ as a soluble species to enable improved dissolution, following Equation 3.

$$Ag_2S\ (s) + 4S_2O_3^{2-} \leftrightarrows 2Ag(S_2O_3)_2^{3-} + S^{2-} \qquad (3)$$

Recent work by Robinson et al. studied the formation of Ag_2S on colliding Ag NPs within solutions of dilute alkaline HS^-.[30] The high insolubility of Ag_2S (pK_{sp} ~ 53.5) resulted in encapsulation of the core Ag and formed either core@shell Ag@Ag_2S NPs or void-containing Ag/Ag_2S NPs, thereby preventing full oxidation. In our experiments, however, the polysulfide layer serves to preconcentrate

sulfide at the electrode surface to where it can take part in the Ag_2S transformation. Further, the presence of sodium thiosulfate as a Lewis base vastly increased the solubility of generated Ag_2S by a factor equivalent to its formation constant ($K_f = 1.7\times10^{13}$); see S12 for details. This may eliminate the precipitated encapsulation effect described by Robinson et al. Our results of increased peak amplitude with polysulfide present could then be explained by the faster reaction of Ag with preconcentrated sulfide, relative to the diffusion-limited arrival of electrolyte in the non-polysulfide condition.

A second mechanism considers recent work by Wang and co-workers who have found that "poor electrical contact" between nano-objects and electrodes can either hinder or eliminate electrochemical activity on the object.[36,37] They suggest that the interaction between the rough NP and bare electrode surfaces may lead to unfavorable configurations for electrical contact. We instead propose that the direct chemical reaction with the polysulfide layer via Equation 2 may be less orientation dependent than landing on a bare electrode and can lead to a higher rate of detected collisions. Alternatively, the adhesive property of the polysulfide layer could also increase the observed collision frequency. It is well-established that Ag NPs do not adhere to the bare Au electrode and can interact with nanosecond scale bursts, faster than the 10 μs electrochemical temporal resolution.[18] The adhesion of these transiently interacting particles would ensure that they produce a measurable signal. Despite the increase, the theoretical diffusion-limited collision rate is still 13x higher than measured, as shown in S13, suggesting that many collisions were undetected.

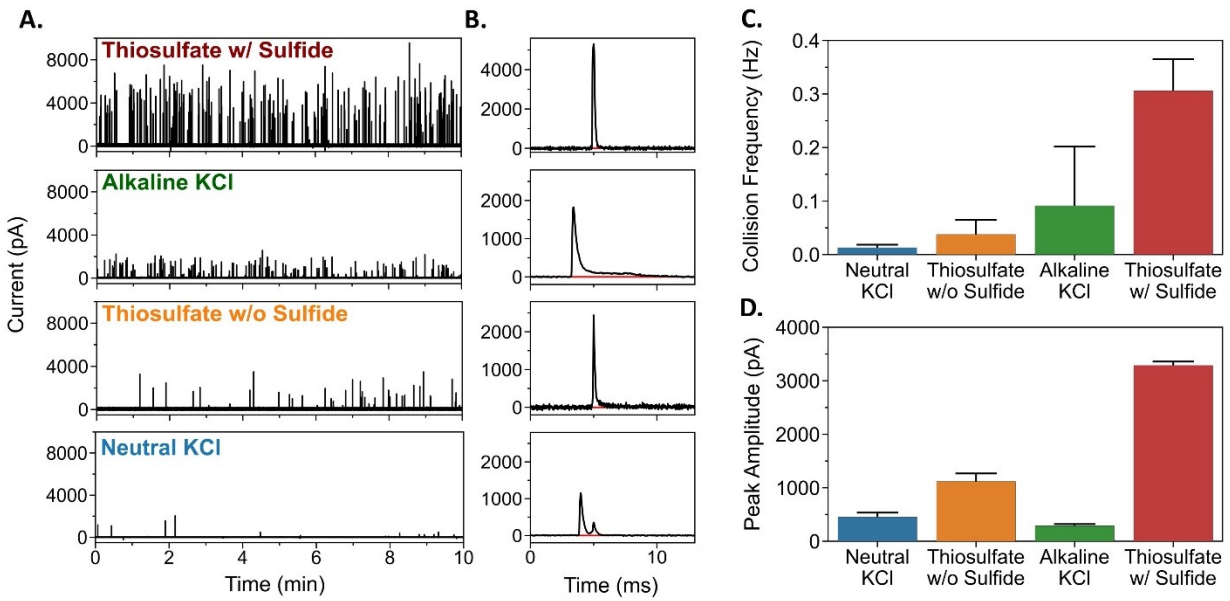

Figure 3: Comparison of Peak Amplitude and Collision Frequency for Four Control Conditions. **(A)** Raw Ag NP Collision traces recorded immediately after injecting Ag NP's. Each trace is recorded with an identical 19 pM Ag NP concentration. Clear differences in collision frequency and peak amplitude are observed. **(B)** Representative peaks under each condition, following baseline adjustment. A horizontal red line is drawn at 0 pA to clearly show where each peak deviates from the baseline, such as for the trailing tail in the Alkaline KCl condition. Further examples of individual peaks are shown in **S8-11**. Note that the y-axis on the "Thiosulfate w/ Thiol" plot is scaled 2 times that of the others. **(C)** The average collision frequency quantified for the first 10 minutes of three traces under each reported condition. The first 10 minutes were selected to avoid influence of particle aggregation. **(D)** The average peak amplitudes for all quantified data. The error bars shown in C, D are for 1 standard deviation above the mean. Specific experimental conditions include: "Thiosulfate w/ Sulfide": 10 mM $Na_2S_2O_3$ 10 mM NaOH on a sulfide-modified Au UME (n = 1943); "Alkaline KCl": 10 mM KCl 10 mM NaOH on a bare Au UME (n = 619); "Thiosulfate w/o Sulfide": 10 mM $Na_2S_2O_3$ 10 mM NaOH on a bare Au UME (n = 143); "Neutral KCl": 20 mM KCl on a bare Au UME (n = 183).

Figure 3 introduces results from two more control conditions that were selected based on their importance to previous Ag NP collision literature. "KCl Control" was collected with 20 mM KCl and is meant to be representative of more classical Ag NP conditions which almost exclusively used neutral single-electrolyte systems.[15–17,38] "Alkaline KCl" was collected with 10 mM KCl 10 mM NaOH in a similar manner to Long and co-worker's work using alkaline phosphate to generate Ag-oxide and promote NP adhesion through strong Au-Ag-oxide contacts.[20,21] Despite our choice to use chloride instead of phosphate, we still observed similar long peak decay events (~10 ms) in **Figure 3b** and **S10** which are suggestive of Ag-oxide formation and slow dissolution. **Figure 3a** shows representative traces of the first 10 minutes under each reported condition with 19 pM 60 nm Ag NPs, while **Figure 3b** shows

representative peaks following baseline adjustment. Averaged collision frequencies and peak amplitudes are shown in **Figures 3c** and **3d**, respectively.

As shown in **Figure 3c**, the thiosulfate with sulfide condition produces the highest collision frequency overall, with a collision rate 25.5x higher than the non-adhesive neutral control. The polysulfide adhesion layer also produces ~ 3.5x higher collision rate than the Ag-oxide adhesive mechanism described by Long and co-workers. Despite both conditions using an adhesive mechanism, we believe this result occurs because the Ag-oxide mechanism depends on the *in-situ* formation of the adhesion layer between the NP and UME. It is possible that some collisions do not form sufficient Ag-oxide to promote adhesion, whereas the adhesion layer is always present in the sulfide condition.

Secondly, we saw that alkaline KCl condition has a 3.3x higher collision frequency than thiosulfate without sulfide, despite maintaining the same NaOH concentration. This observation can be explained by considering the Lewis base identity of thiosulfate. The solubility of Ag oxide is significantly increased in its presence, where the equilibrium constant K (calculated by multiplying K_{sp} x K_f) of Ag-oxide in alkaline thiosulfate is 3.2×10^{5} (compared to the value of 1.9×10^{-8} in water[39]). More complete dissolution of Ag-oxide eliminates its adhesive contacts and lowers the rate of detected collisions for the alkaline thiosulfate condition in the absence of the sulfide adhesion layer.

Figure 3d compares the average peak amplitude for all data collected under the respective solution conditions. The peak amplitude is indicative of the flux of transferred electrons and is correlated with the rate of electrochemical oxidation. We find that both thiosulfate-containing electrolyte conditions produces the highest peak amplitudes. This phenomenon is again due to the extreme solubility of Ag-thiosulfate oxidation products accommodating the massive influx of Ag^{+} in the solution volume surrounding the NP. On the other hand, the basic KCl condition produced the lowest amplitude peaks due to the dominant formation of Ag-oxide which reportedly undergoes slow dissolution.

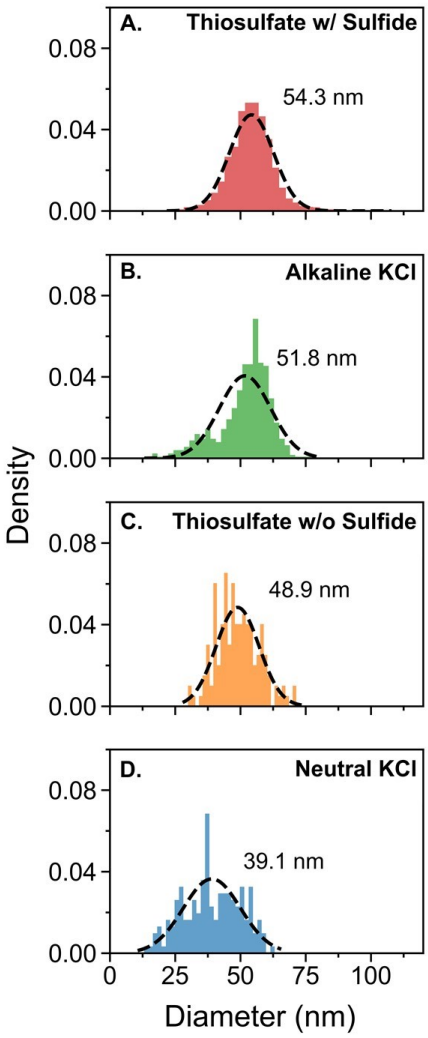

Figure 4: Sulfide-Modified Au UME Increases Oxidation Efficiency. The equivalent spherical diameter of 60 nm Ag NP's were calculated using the integrated charge and Equation 4 under various Ag NP electrolyte conditions. Specific experimental conditions include: **(A)** 10 mM $Na_2S_2O_3$ 10 mM NaOH on a sulfide-modified Au UME (n = 1943); **(B)** 10 mM KCl 10 mM NaOH on a bare Au UME (n = 619); **(C)** 10 mM $Na_2S_2O_3$ 10 mM NaOH on a bare Au UME (n = 143); **(D)** 20 mM KCl on a bare Au UME (n = 183). Each distribution was fit using a Gaussian Maximum Likelihood Estimation (MLE), including all data. The values reported on each plot are the mean of the Gaussian fit.

Effects on Oxidation Efficiency from the Polysulfide Modified Electrode. We next investigated the influence of the sulfide adhesion layer on the integrated charge for each NP collision event. With Equation 4, the charge (Q) is used to estimate the radius, r, of an equivalent spherical particle.[5] Here, n = 1 electron, A_r is the atomic mass of Ag (107.87 g mol^{-1}), F is the Faraday constant (96 485 C mol^{-1}), and ρ is the density of silver (10.49 g cm^{-3}).

$$r = \left(\frac{3A_r Q}{4\pi n F \rho}\right)^{1/3} \quad (4)$$

In **Figure 4**, we show the distributions of equivalent spherical NP diameters calculated with 60 nm Ag NP collision data using the same four control conditions as **Figure 3**. Each distribution was fit with a Gaussian function using the maximum likelihood estimate (MLE), where the mean of the fit is labeled on each respective plot.

We find that the Au-sulfide condition produces the largest estimated diameter of 54.3 nm compared to 51.8 nm for the alkaline KCl control, 48.9 nm for the non-sulfide thiosulfate, and 39.1 nm for the neutral KCl solution. Results suggest that larger oxidation efficiencies are obtained for conditions that better promote NP adhesion. This idea is consistent with initial multipeak papers which cited diffusion of the NP away from the electrode as the main mechanism for incomplete oxidation.[15–17] Longer residence times on the electrode surface allow for ongoing dissolution of generated Ag salts and continued Ag oxidation.

One remarkable observation from **Figure 4b** is that the distribution of oxidation efficiencies for the alkaline KCl condition is bimodal. These trailing results toward smaller diameters are consistent with previous literature for 60 and 65 nm Ag NP's in alkaline phosphate, though have not been discussed explicitly.[20,21] Here, the larger half of the bimodal distribution is centered at 55.1 nm, yielding results similar to those using the adhesive Au-sulfide condition. However, the smaller half of the distribution is centered at 33.6 nm and is more similar to the non-adhesive neutral KCl control condition. Given that oxidation efficiency is related to adhesive strength, these smaller events may result from collisions that fail to form sufficient Ag-oxide *in-situ* to promote adhesion, thereby resulting in quick incomplete events. Nonetheless, the existence of the second distribution centered at 33.6 nm pulls the MLE Gaussian fit lower to an overall average of 51.8 nm and a less accurate quantitative result.

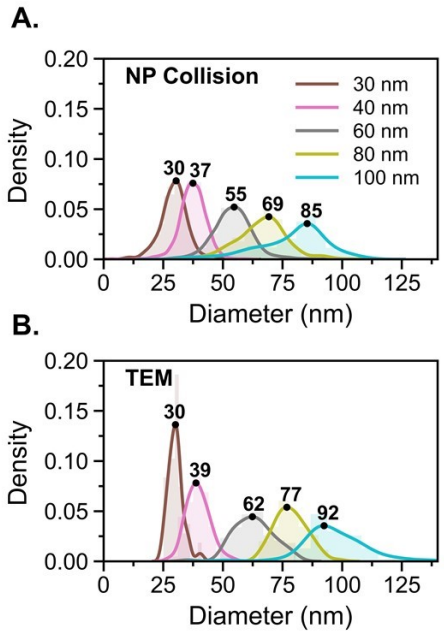

Figure 5: Quantitation of Ag NP Diameter for NP Collision vs. TEM. **(A)** The sulfide-modified Au UME condition (10 mM $Na_2S_2O_3$ 10 mM NaOH) was used to quantify equivalent spherical diameter for Ag Collision data for NP's with diameters 30, 40, 60, 80, 100 nm using the integrated charge and Equation 4. (n = 722, 1498, 1943, 786, 557 for 30, 40, 60, 80, 100 nm Ag NP collision data, respectively). **(B)** Equivalent spherical diameters of Ag NP's were estimated using the 2D projection method on TEM data, as described in S5. (n = 67, 63, 85, 83, 66 for 30, 40, 60, 80, 100 nm TEM data, respectively.) We chose to plot the KDE of each distribution to clearly show the leading and trailing tails of each population, rather than forcing a symmetrical Gaussian fit. The maximum point of each KDE distribution is labeled. Example representative NP collision traces for each population are shown in **S7**.

In **Figure 5**, we investigate particle sizing results for 30, 40, 60, 80, and 100 nm Ag NPs using the Au-polysulfide oxidative collision method compared with TEM. We chose to plot data in terms of probability density fit with the kernel density estimate (KDE) to better show the distribution shape rather than forcing a symmetrical Gaussian fit. When comparing the maximum density values of each population, we observe identical equivalent spherical diameters for 30 nm Ag NPs with more significant deviations for larger particle sizes.

Previous Ag NP collision literature has treated TEM as an accurate volumetric reference to determine whether full NP oxidation had occurred.[20] However, researchers should be cautious when making this comparison. The process of volumetric sizing with TEM via the 2D projection method quantifies the area of a 2D NP slice and uses the measured value to calculate the radius of an equivalent

sphere, as described in **S5**. Thus, only perfect spheres produce perfectly accurate volumetric measurements.

An important study by Attota et al. explored the error of the 2D projection method by simulating 3D NP models of known volume with different degrees of surface roughness and non-sphericity.[40] They found that rough, faceted, and oblong NP geometries can have their volume overestimated by up to 18% using the same 2D projection method applied in TEM data analysis. Note that a constant percent overestimation leads to larger numerical differences for increased NP size. While this reference was published in 2016, we emphasize its importance since previous Ag NP collision papers have treated TEM volumetric sizing as ground truth and expressed the desire to exactly match these results. This quest is unproductive for large (>50 nm) quasi-spherical Ag NPs since the application of TEM with the 2D projection method will consistently overestimate the equivalent spherical diameter. A more realistic strategy would be to compare the percent difference between TEM and NP collision to ensure that it is within an appropriate error margin.

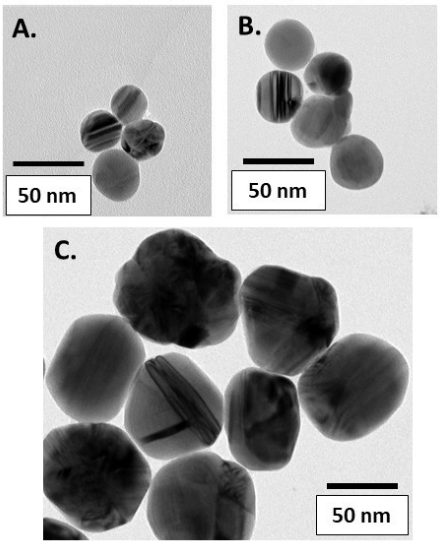

Figure 6. Representative TEM Images of Quasi-Spherical Ag NP Sample Populations. Samples include 30 nm **(A)**, 40 nm **(B)**, and 80 nm **(C)** populations, as purchased from the commerical supplier. Irregularity in the form of facets and non-sphericity appears to increase with particle size. Images are scaled to the same scale bar length to better compare particle geometry. Additional representative TEM images for other NP sizes are shown in **S6**.

Indeed, our TEM results in **Figure 6** and **S6** confirm the presence of such faceted and oblong particles, especially for sizes greater than 40 nm diameter. The percent error between the maximum density values for our equivalent spherical diameters derived using NP collisions and TEM in **Figure 5** exist as 5.1%, 11.3%, 10.4%, and 7.6% for the 40, 60, 80, and 100 nm Ag NP populations, respectively. Since these values are well within the 18% volumetric error margin of the 2D projection method, it remains possible that full particle oxidation is occurring. However, given that the error margin is relatively large, the use of additional analytical techniques could help to validate this result. One strategy would be to obtain a more accurate volumetric reference using a method such as electron tomography,[12,41] but such measurements would be prohibitively expensive. Alternatively, correlated imaging strategies may enable observation of the physical processes which occur subsequent to each oxidative spike.[42,43]

Lastly, we observed that our 80 and 100 nm Ag NP collision results in **Figure 5a** show trailing distributions toward smaller particle sizes, indicative of incomplete oxidation. We believe the NPs in the trailing population are still adhered to the sulfide layer, due to the long durations of the events. For example, 100 nm events with less than 65 nm equivalent diameters had mean durations of 8.6 ms. One proposed mechanism for this process is that large Ag NPs may consume the local polysulfide adhesion layer and convert it to soluble Ag_2S with the aid of bulk thiosulfate. Eliminating the adhesive contact may then detach the NP and prevent further oxidation. Since the trailing peaks only account for a small percentage of the total number of events, the variable thickness of the polysulfide film could account for this inconsistent behavior. Further investigation with correlated imaging would better validate the mechanism that complicates the complete oxidation of large Ag NP sizes.

Conclusions.

In summary, our study has shown the collision, adhesion, and oxidation behavior of single Ag NPs on a gold microelectrode can be greatly promoted by an ultrathin layer of polysulfide. The polysulfide layer is formed on the gold surface from the oxidation of sodium thiosulfate in an alkaline solution environment. The polysulfide film can serve both as an effective adhesive surface to enhance the

sticking probability for colliding Ag NPs and as a promoter for enhancing the kinetics of Ag oxidation. Rapid NP dissolution was seen by the presence of bulk sodium thiosulfate which served as a Lewis base to vastly improve the solubility of Ag_2S and Ag^+. Our collision results with 60 nm Ag NPs suggest the presence of sulfide and bulk thiosulfate resulted in a 25x increase in collision frequency, 3x increase in peak amplitude, and more complete oxidation. We further applied this methodology toward quantitative volumetric detection of quasi-spherical 30, 40, 60, 80, and 100 nm Ag NP populations and found reasonable evidence that full oxidation occurred for all NP sizes. However, we emphasize that the use of quasi-spherical NPs leads to an over-estimation of TEM equivalent spherical diameters, an artifact of TEM data analysis that is often overlooked in this field. Despite full oxidation being predominantly observed for 80 and 100 nm Ag NPs, we propose that consumption of the local polysulfide layer led to trailing distributions of estimated particle size. We believe that the use of a non-consumable adhesive layer applied to the electrode surface may resolve this issue and lead to more uniform and quantitative sizing for large Ag NPs. Lastly, we expect the observed NP adhesive properties of polysulfide to benefit other NP collision systems via promotion of more effective NP-UME electrical contact.

ASSOCIATED CONTENT

Supporting Information

Python program for data analysis, more details on experimental conditions used for NP collision, cyclic voltammetry in alkaline thiosulfate, NP volume estimate with 2D projection methods, TEM images, representative NP collision events in various conditions, equilibrium describing the improved solubility of Ag salts from a Lewis base, calculation of the theoretical collision frequency, investigation of Au oxide formation during the polysulfide passivation process, and measurement of the electroactive surface area of bare and polysulfide removed electrodes. This material is available free of charge via the Internet at http://pubs.acs.org.

AUTHOR INFORMATION

Corresponding Author

zhang@chem.washington.edu (BZ)

Notes

The authors declare no competing financial interests.

Acknowledgements.

This work was supported by the National Science Foundation (CHE-1904426). Part of this work was conducted at the Molecular Analysis Facility, a National Nanotechnology Coordinated Infrastructure (NNCI) site at the University of Washington, which is supported in part by funds from the National Science Foundation (awards NNCI-2025489, NNCI-1542101), the Molecular Engineering & Sciences Institute, and the Clean Energy Institute.

References:

(1) Goines, S.; Dick, J. E. Review—Electrochemistry's Potential to Reach the Ultimate Sensitivity in Measurement Science. *J. Electrochem. Soc.* **2020**, *167* (3), 037505. https://doi.org/10.1149/2.0052003jes.

(2) Patrice, F. T.; Qiu, K.; Ying, Y.; Long, Y. Single Nanoparticle Electrochemistry. *Annu. Rev. Anal. Chem.* **2019**, *12*, 347–370.

(3) Quinn, B. M.; Van't Hof, P. G.; Lemay, S. G. Time-Resolved Electrochemical Detection of Discrete Adsorption Events. *J. Am. Chem. Soc.* **2004**, *126*, 8360–8361. https://doi.org/10.1021/ja0478577.

(4) Xiao, X.; Bard, A. J. Observing Single Nanoparticle Collisions at an Ultramicroelectrode by Electrocatalytic Amplification. *J. Am. Chem. Soc.* **2007**, *129*, 9610–9612. https://doi.org/10.1021/ja072344w.

(5) Zhou, Y. G.; Rees, N. V.; Compton, R. G. The Electrochemical Detection and Characterization of Silver Nanoparticles in Aqueous Solution. *Angew. Chemie - Int. Ed.* **2011**, *50*, 4219–4221. https://doi.org/10.1002/anie.201100885.

(6) Sokolov, S. V.; Eloul, S.; Katelhon, E.; Batchelor-Mcauley, C.; Compton, R. G. Electrode – Particle Impacts : A Users Guide. *Phys. Chem. Chem. Phys.* **2017**, *19*, 28–43. https://doi.org/10.1039/C6CP07788A.

(7) Karimi, A.; Hayat, A.; Andreescu, S. Biomolecular Detection at SsDNA-Conjugated Nanoparticles by Nano-Impact Electrochemistry. *Biosens. Bioelectron.* **2017**, *87*, 501–507. https://doi.org/10.1016/j.bios.2016.08.108.

(8) Zhang, X. F.; Liu, Z. G.; Shen, W.; Gurunathan, S. Silver Nanoparticles: Synthesis, Characterization, Properties, Applications, and Therapeutic Approaches. *Int. J. Mol. Sci.* **2016**, *17*, 1534. https://doi.org/10.3390/ijms17091534.
(9) Iravani, S.; Korbekandi, H.; Mirmohammadi, S. V; Zolfaghari, B. Synthesis of Silver Nanoparticles: Chemical, Physical and Biological Methods. *Res. Pharm. Sci.* **2014**, *9*, 385–406.
(10) Albanese, A.; Tang, P. S.; Chan, W. C. W. The Effect of Nanoparticle Size, Shape, and Surface Chemistry on Biological Systems. *Annu. Rev. Biomed. Eng.* **2012**, *14*, 1–16. https://doi.org/10.1146/annurev-bioeng-071811-150124.
(11) Nel, A.; Xia, T.; Mädler, L.; Li, N. Toxic Potential of Materials at the Nanolevel. *Science (80-.).* **2006**, *311*, 622–627. https://doi.org/10.1126/science.1114397.
(12) Little, C. A.; Batchelor-Mcauley, C.; Young, N. P.; Compton, R. G. Shape and Size of Non-Spherical Silver Nanoparticles: Implications for Calculating Nanoparticle Number Concentrations. *Nanoscale* **2018**, *10*, 15943–15947. https://doi.org/10.1039/c8nr06062b.
(13) Albrecht, W.; Bals, S. Fast Electron Tomography for Nanomaterials. *J. Phys. Chem. C* **2020**, *124*, 27276–27286. https://doi.org/10.1021/acs.jpcc.0c08939.
(14) Defnet, P. A.; Anderson, T. J.; Zhang, B. Stochastic Collision Electrochemistry of Single Silver Nanoparticles. *Curr. Opin. Electrochem.* **2020**, *22*, 129–135. https://doi.org/10.1016/j.coelec.2020.06.004.
(15) Ma, W.; Ma, H.; Chen, J. F.; Peng, Y. Y.; Yang, Z. Y.; Wang, H. F.; Ying, Y. L.; Tian, H.; Long, Y. T. Tracking Motion Trajectories of Individual Nanoparticles Using Time-Resolved Current Traces. *Chem. Sci.* **2017**, *8* (3), 1854–1861. https://doi.org/10.1039/c6sc04582k.
(16) Oja, S. M.; Robinson, D. A.; Vitti, N. J.; Edwards, M. A.; Liu, Y.; White, H. S.; Zhang, B. Observation of Multipeak Collision Behavior during the Electro-Oxidation of Single Ag Nanoparticles. *J. Am. Chem. Soc.* **2017**, *139*, 708–718. https://doi.org/10.1021/jacs.6b11143.
(17) Ustarroz, J.; Kang, M.; Bullions, E.; Unwin, P. R. Impact and Oxidation of Single Silver Nanoparticles at Electrode Surfaces: One Shot versus Multiple Events. *Chem. Sci.* **2017**, *8*, 1841–1853. https://doi.org/10.1039/c6sc04483b.
(18) Robinson, D. A.; Liu, Y.; Edwards, M. A.; Vitti, N. J.; Oja, S. M.; Zhang, B.; White, H. S. Collision Dynamics During the Electrooxidation of Individual Silver Nanoparticles. *J. Am. Chem. Soc.* **2017**, *139*, 16923–16931. https://doi.org/10.1021/jacs.7b09842.
(19) Sun, L.; Wang, W.; Chen, H. Y. Dynamic Nanoparticle-Substrate Contacts Regulate Multi-Peak Behavior of Single Silver Nanoparticle Collisions. *ChemElectroChem* **2018**, *5*, 2995–2999. https://doi.org/10.1002/celc.201800640.
(20) Ma, H.; Chen, J. F.; Wang, H. F.; Hu, P. J.; Ma, W.; Long, Y. T. Exploring Dynamic Interactions of Single Nanoparticles at Interfaces for Surface-Confined Electrochemical Behavior and Size Measurement. *Nat. Commun.* **2020**, *11*, 1–9. https://doi.org/10.1038/s41467-020-16149-0.
(21) Hafez, M. E.; Ma, H.; Peng, Y.; Ma, W.; Long, Y. Correlated Anodic–Cathodic Nanocollision Events Reveal Redox Behaviors of Single Silver Nanoparticles. *J. Phys. Chem. Lett.* **2019**, *10*, 3276–3281. https://doi.org/10.1021/acs.jpclett.9b01369.
(22) Zelinsky, A. G. RDE Study of Thiosulfate Oxidation on Gold. *J. Electroanal. Chem.* **2014**, *735*, 111–114. https://doi.org/10.1016/j.jelechem.2014.10.018.
(23) Krause, K. J.; Adly, N.; Yakushenko, A.; Schnitker, J.; Mayer, D.; Offenhäusser, A.; Wolfrum, B. Influence of Self-Assembled Alkanethiol Monolayers on Stochastic Amperometric On-Chip Detection of Silver Nanoparticles. *Anal. Chem.* **2016**, *88*, 3632–3637. https://doi.org/10.1021/acs.analchem.5b04306.
(24) Bell, R. A.; Kramer, J. R. Structural Chemistry and Geochemistry of Silver-Sulfur Compounds: Critical Review. *Environ. Toxicol. Chem.* **1999**, *18*, 9–22. https://doi.org/10.1897/1551-5028(1999).
(25) Pakiari, A. H.; Jamshidi, Z. Nature and Strength of MS Bonds (M = Au, Ag, and Cu) in Binary Alloy Gold Clusters. *J. Phys. Chem. A* **2010**, *114*, 9212–9221. https://doi.org/10.1021/jp100423b.
(26) Pollok, N. E.; Rabin, C.; Smith, L.; Crooks, R. M. Orientation-Controlled Bioconjugation of

Antibodies to Silver Nanoparticles. *Bioconjugate Chem.* **2019**, *30*, 3078–3086. https://doi.org/10.1021/acs.bioconjchem.9b00737.
(27) Marchioni, M.; Battocchio, C.; Joly, Y.; Gateau, C.; Nappini, S.; Pis, I.; Delangle, P.; Michaud-Soret, I.; Deniaud, A.; Veronesi, G. Thiolate-Capped Silver Nanoparticles: Discerning Direct Grafting from Sulfidation at the Metal-Ligand Interface by Interrogating the Sulfur Atom. *J. Phys. Chem. C* **2020**, *124*, 13467–13478. https://doi.org/10.1021/acs.jpcc.0c03388.
(28) Gan, W.; Xu, B.; Dai, H. L. Activation of Thiols at a Silver Nanoparticle Surface. *Agnew. Chem. Int. Ed.* **2011**, *50*, 6622–6625. https://doi.org/10.1002/anie.201101430.
(29) Love, J. C.; Estroff, L. A.; Kriebel, J. K.; Nuzzo, R. G.; Whitesides, G. M. Self-Assembled Monolayers of Thiolates on Metals as a Form of Nanotechnology. *Chem. Rev.* **2005**, *105*, 1103-1170. https://doi.org/10.1021/cr0300789.
(30) Robinson, D. A.; White, H. S. Electrochemical Synthesis of Individual Core@Shell and Hollow Ag/Ag_2S Nanoparticles. *Nano Lett.* **2019**, *19*, 5612–5619. https://doi.org/10.1021/acs.nanolett.9b02144.
(31) Woods, R.; Hope, G. A.; Watling, K. M.; Jeffrey, M. I. A Spectroelectrochemical Study of Surface Species Formed in the Gold/Thiosulfate System. *J. Electrochem. Soc.* **2006**, *153*, D105. https://doi.org/10.1149/1.2195889.
(32) Gao, X.; Zhang, Y.; Weaver, M. J. Adsorption and Electrooxidative Pathways for Sulfide on Gold As Probed by Real-Time Surface-Enhanced Raman Spectroscopy. *Langmuir* **1992**, *8*, 668–672. https://doi.org/10.1021/la00038a060.
(33) Zelinsky, A. G. Anode Current on Gold in Mixed Thiosulfate-Sulfite Electrolytes. *Electrochim. Acta* **2015**, *154*, 315–320. https://doi.org/10.1016/j.electacta.2014.12.097.
(34) Lay, M. D.; Varazo, K.; Stickney, J. L. Formation of Sulfur Atomic Layers on Gold from Aqueous Solutions of Sulfide and Thiosulfate: Studies Using EC-STM, UHV-EC, and TLEC. *Langmuir* **2003**, *19*, 8416–8427. https://doi.org/10.1021/la034474y.
(35) Pedraza, A. M.; Villegas, I.; Freund, P. L.; Chornik, B. Electro-Oxidation of Thiosulphate Ion on Gold. Study by Means of Cyclic Voltammetry and Auger Electron Spectroscopy. *J. Electroanal. Chem.* **1988**, *250*, 443–449. https://doi.org/10.1016/0022-0728(88)85183-0.
(36) Jiang, W.; Wei, W.; Yuan, T.; Liu, S.; Niu, B.; Wang, H.; Wang, W. Tracking the Optical Mass Centroid of Single Electroactive Nanoparticles Reveals the Electrochemically Inactive Zone. *Chem. Sci.* **2021**, *12*, 8556–8562. https://doi.org/10.1039/d1sc01623g.
(37) Wei, W.; Yuan, T.; Jiang, W.; Gao, J.; Chen, H.-Y.; Wang, W. Accessing the Electrochemical Activity of Single Nanoparticles by Eliminating the Heterogeneous Electrical Contacts. *J. Am. Chem. Soc.* **2020**, *142*, 14307–14313. https://doi.org/10.1021/jacs.0c06171.
(38) Ngamchuea, K.; Clark, R. O. D.; Sokolov, S. V; Young, N. P.; Batchelor-Mcauley, C.; Compton, R. G. Single Oxidative Collision Events of Silver Nanoparticles : Understanding the Rate-Determining Chemistry. *Chem. Eur. J.* **2017**, *23*, 16085–16096. https://doi.org/10.1002/chem.201703591.
(39) Sauls, F. C. A Simple Determination of the Ag2O Solubility Product by Potentiometric Determinations of Both Ag+1 and OH-1. *J. Chem. Educ.* **2013**, *90*, 1212–1214. https://doi.org/10.1021/ed300586g.
(40) Attota, R. K.; Liu, E. C. Volume Determination of Irregularly-Shaped Quasi-Spherical Nanoparticles. *Anal. Bioanal. Chem.* **2016**, *408*, 7897–7903. https://doi.org/10.1007/s00216-016-9909-x.
(41) Van Doren, E. A. F.; De Temmerman, P. J. R. H.; Francisco, M. A. D.; Mast, J. Determination of the Volume-Specific Surface Area by Using Transmission Electron Tomography for Characterization and Definition of Nanomaterials. *J. Nanobiotechnology* **2011**, *9*, 17. https://doi.org/10.1186/1477-3155-9-17.
(42) Patel, A. N.; Martinez-marrades, A.; Brasiliense, V.; Koshelev, D.; Besbes, M.; Kuszelewicz, R.; Combellas, C.; Tessier, G.; Kanoufi, F. Deciphering the Elementary Steps of Transport-Reaction Processes at Individual Ag Nanoparticles by 3D Superlocalization Microscopy. *Nano Lett.* **2015**,

15, 6454–6463. https://doi.org/10.1021/acs.nanolett.5b02921.
(43) Sundaresan, V.; Monaghan, J. W.; Willets, K. A. Monitoring Simultaneous Electrochemical Reactions with Single Particle Imaging. *ChemElectroChem* **2018**, *5*, 3052–3058. https://doi.org/10.1002/celc.201800715.

For Table of Contents Only